Molecular Biology of the Cell
Vol. 19, 2465–2475, June 2008

Deficiency of Zonula Occludens-1 Causes Embryonic Lethal Phenotype Associated with Defected Yolk Sac Angiogenesis and Apoptosis of Embryonic Cells

Tatsuya Katsuno,[*†] Kazuaki Umeda,[‡§‖] Takeshi Matsui,[*¶] Masaki Hata,[§#] Atsushi Tamura,[*] Masahiko Itoh,[‡@] Kosei Takeuchi,[†] Toshihiko Fujimori,[††] Yo-ichi Nabeshima,[††] Tetsuo Noda,[‡‡] Shoichiro Tsukita,[‡] and Sachiko Tsukita[*]**

[*]Laboratory of Biological Science, Graduate School of Frontier Biosciences, and Graduate School of Medicine, Osaka University, Osaka 565-0871, Japan; [†]Department of Biological Science, Nagoya University Graduate School of Science, Nagoya 464-8602, Japan; [‡]Department of Cell Biology, Faculty of Medicine, Kyoto University, Kyoto 606-8501, Japan; [§]KAN Research Institute, Inc., Kobe MI R&D Center, Kobe 650-0047, Japan; [††]Department of Pathology and Tumor Biology, Graduate School of Medicine, Kyoto University, Kyoto 606-8501, Japan; and [‡‡]Department of Cell Biology, Cancer Institute of the Japanese Foundation for Cancer Research, Tokyo 135-8550, Japan

Submitted December 6, 2007; Revised February 25, 2008; Accepted March 10, 2008
Monitoring Editor: Keith Mostov

Zonula occludens (ZO)-1/2/3 are the members of the TJ-MAGUK family of membrane-associated guanylate kinases associated with tight junctions. To investigate the role of ZO-1 (encoded by *Tjp1*) in vivo, ZO-1 knockout (*Tjp1*$^{-/-}$) mice were generated by gene targeting. Although heterozygous mice showed normal development and fertility, delayed growth and development were evident from E8.5 onward in *Tjp1*$^{-/-}$ embryos, and no viable *Tjp1*$^{-/-}$ embryos were observed beyond E11.5. *Tjp1*$^{-/-}$ embryos exhibited massive apoptosis in the notochord, neural tube area, and allantois at embryonic day (E)9.5. In the yolk sac, the ZO-1 deficiency induced defects in vascular development, with impaired formation of vascular trees, along with defective chorioallantoic fusion. Immunostaining of wild-type embryos at E8.5 for ZO-1/2/3 revealed that ZO-1/2 were expressed in almost all embryonic cells, showing tight junction-localizing patterns, with or without ZO-3, which was confined to the epithelial cells. ZO-1 deficiency depleted ZO-1-expression without influence on ZO-2/3 expression. In *Tjp1*$^{+/+}$ yolk sac extraembryonic mesoderm, ZO-1 was dominant without ZO-2/3 expression. Thus, ZO-1 deficiency resulted in mesoderms with no ZO-1/2/3, associated with mislocalization of endothelial junctional adhesion molecules. As a result, angiogenesis was defected in *Tjp1*$^{-/-}$ yolk sac, although differentiation of endothelial cells seemed to be normal. In conclusion, ZO-1 may be functionally important for cell remodeling and tissue organization in both the embryonic and extraembryonic regions, thus playing an essential role in embryonic development.

INTRODUCTION

In multicellular organisms, cell–cell adhesion is critical for development and morphogenesis. Various types of cell–cell adhesion-related molecules have been identified, and evidence has accumulated that their expression and functions are critically regulated in a spatiotemporally highly organized way (Tsukita *et al*., 2001; Halbleib and Nelson, 2006). In general, cell–cell adhesion molecules are integral membrane proteins that associate with peripheral membrane proteins to regulate and integrate cell–cell adhesion-related phenomena. Zonula occludens (ZO)-1 is a founding member of membrane-associated guanylate kinase (MAGUK) family proteins of tight junctions (TJs), composed of three postsynaptic density 95/disc-large/ZO-1 (PDZ) domains, a Src homology 3 domain, a guanylate kinase (GUK) domain, an acidic domain, and an actin binding region (Itoh *et al*., 1993; Willott *et al*., 1993; Jesaitis and Goodenough, 1996; Haskins *et al*., 1998). It was first defined as an antigen for monoclonal antibodies that recognized TJs in epithelial cells, and it was

This article was published online ahead of print in *MBC in Press* (http://www.molbiolcell.org/cgi/doi/10.1091/mbc.E07–12–1215) on March 19, 2008.

Present addresses: [‖] Department of Molecular Pharmacology, Graduate School of Medical Science, Kumamoto University, Honjo, Kumamoto 860-8556, Japan; [¶] Medical Top Track Program, Medical Research Institute, Tokyo Medical and Dental University, 1-5-45 Yushima, Bunkyo-ku, Tokyo 135-8550, Japan; [#] Department of Pathology, Hyogo College of Medicine, 4-11 Mukogawa-cho, Nishinomiya, Hyogo 663-8501, Japan; [@] Department of Molecular and Cell Biology, Institute of Medical Science, Dokkyo Medical University, Shimotsuga-gun, Tochigi, 321-0293 Japan; [**] Department of Anatomy and Developmental Biology, Graduate School of Medical Science, Kyoto Prefectural University of Medicine, Kawaramachi-Hirokoji, Kamigyo-ku, Kyoto 602-8566, Japan.

Address correspondence to: Sachiko Tsukita (atsukita@biosci.med.osaka-u.ac.jp).

Abbreviations used: MAGUK, membrane-associated guanylate kinase; TJ, tight junction; AJ, adherens junction; PDZ, postsynaptic density 95/disc-large/zona occludens; ZA, zonula adherens; ZO, zonula occludens.

subsequently revealed as a peripheral membrane protein with a molecular mass of 220 kDa, which underlied the cytoplasmic surface of plasma membranes of TJs (Stevenson *et al*., 1986). Evidence has accumulated that in epithelial cells, ZO-1 is exclusively located at TJs, but when TJs are not formed, it is concentrated in adherens junctions (AJs) (Itoh *et al*., 1993, 1999; Furuse *et al*., 1994; Fanning *et al*., 1998; Bazzoni *et al*., 2000). In nonepithelial cells without TJs such as cardiac muscle cells and fibroblasts, ZO-1 is colocalized with cadherins to form AJs (Itoh *et al*., 1999). ZO-2 was identified as a 160-kDa protein that was coimmunoprecipitated with ZO-1 from cell lysates (Gumbiner *et al*., 1999). A phosphorylated 130-kDa protein that coimmunoprecipitated with ZO-1 was ZO-3 (Balda *et al*., 1993). ZO-2 behaved similarly to ZO-1, although with slight functional differences, whereas ZO-3 was much more distinct from ZO-1/2, only detected in epithelia (Inoko *et al*., 2003), and localized to TJs in a ZO-1/2–dependent way (Wittchen *et al*., 1999). The molecular basis underlying this distribution is reported that ZO-1 binds to AJ-constitutive peripheral membrane proteins, such as α-catenin, afadin, and actin, via the N-terminal, N-terminal, and C-terminal half-domains of ZO-1, respectively, thus being linked to the adhesion molecules of AJs such as cadherin and nectin (Itoh *et al*., 1993, 1997; Yamamoto *et al*., 1997; Fanning *et al*., 1998). Conversely, ZO-1 directly binds to adhesion molecules of TJs such as claudins and occludin by PDZ-1 and GUK domains of ZO-1, respectively (Mitic and Anderson, 1998; Gonzalez-Mariscal *et al*., 2000). The functional roles of ZO-1 in AJs and TJs are supposed to be coordinated by a proper switching mechanism, as a junctional organizer.

In the ZO-1-knockout (KO)/ZO-2-knockdown (KD) epithelial Eph4 cells, in addition to the formation of liner epithelial-typed AJs (zonula adherens [ZA]) being impeded, the formation of claudin-based linear TJs (zonula occludens) was abolished (Umeda *et al*., 2006). It was recently revealed that when epithelial ZA was formed from primordial AJs, ZO-1/2 regulated the time course of the formation of ZA in a rac-dependent way (Ikenouchi *et al*., 2007). Although ZO-3 supposedly played a role distinct from that of ZO-1/2, ZO-3 deficiency produced no phenotypes in cells and mice (Adachi *et al*., 2006). Thus, ZO-1 and its relative ZO-2 are among the factors that play critical roles in the formation and maintenance of ZA and ZO of the cell–cell adhesion apparatus (Umeda *et al*., 2004, 2006; Hernandez *et al*., 2007; Ikenouchi *et al*., 2007).

In this study, we generated ZO-1–deficient mice to explore the function of ZO-1 in vivo. ZO-1–deficient mice died at the embryonic (E) stage around day 10.5, with embryonic and extraembryonic defects. As embryonic defects, an absence of turning was noted in almost all embryos in the macroscopic and microscopic views, and the neural tube and notochord areas as well as allantois were found to be disorganized due to apoptosis. As a yolk sac extraembryonic defect, angiogenesis seemed to be impaired in ZO-1–deficient mice, affecting embryonic development. These results demonstrate a critical role for ZO-1 in early embryonic development due to both of embryonic and extraembryonic effects, suggesting the important role of cell–cell adhesive junctions in tissue organization and remodeling.

MATERIALS AND METHODS

Antibodies

Mouse and rat anti-ZO-1 monoclonal antibody (mAb) (Ioth *et al*., 1993; Kitajiri *et al*., 2004), rabbit anti-ZO-3 polyclonal antibody (pAb) (Inoko *et al*., 2003), rat anti-occludin mAb (Saitou *et al*., 1997), and rabbit anti-junctional adhesion molecule (JAM)-A pAb (Komiya *et al*., 2005), rabbit anti-claudin-6 pAb (Morita *et al*., 1999) and rat anti-cingulin mAb (Ohnishi *et al*., 2004) were used as described previously. Rat anti-mouse E-cadherin mAb (ECCD2) was generously provided by Dr. M. Takeichi (Center for Developmental Biology, Kobe, Japan). Rabbit anti-afadin pAb was generated using amino acids 1447–1822 of afadin. Antibodies for goat anti-ZO-2 and anti-VE-cadherin pAb (Santa Cruz Biotechnology, Santa Cruz, CA), rat anti-platelet/endothelial cell adhesion molecule (PECAM)-1 mAb (BD Biosciences PharMingen, San Diego, CA), rabbit anti-caspase-3 pAb (Cell Signaling Technology, Danvers, MA), rabbit anti-α-catenin and anti-β-catenin pAb (Sigma Chemical, Poole, Dorset, United Kingdom), and rabbit anti-myosin-2B (MHC-B) pAb (Covance Research Products, Princeton, NJ), as well as rat anti-Ki-67 pAb (Dako Denmark A/S, Glostrup, Denmark), rhodamine-phalloidin (Cytoskeleton, Denver, CO), and 4,6-diamidino-2-phenylindole (DAPI) (Nakarai Tesque, Kyoto, Japan) were purchased commercially.

Generation of ZO-1 Knockout Mice

The λ phage 129/Sv mouse genomic library was screened using mouse ZO-1 cDNA fragments as a probe. For the gene targeting of embryonic stem (ES) cells, a 5.1-kb PstI–BsrDI fragment and a 1.7-kb PvuII fragment were ligated to the targeting vector cassette. The targeting vector containing the β-geo was linearized at a unique SacII site located at the 5′ end of the 5′ homologous fragment, and then 4×10^7 ES cells were electroporated with 100 μg of linearized targeting vector DNA using a Gene Pulser (Bio-Rad, Hercules, CA) set at 400 V and 25 μF. Cells were plated on feeder cells in DMEM supplemented with 20% fetal calf serum for 48 h, followed by selection with 100 μg/ml Geneticin (G-418). After 8 d, the G-418–resistant colonies were picked up and screened by Southern blotting with the 3′ external probe. Correctly targeted clones were identified by additional 8.6-kb band together with the 21-kb band of the wild-type allele. Tail biopsy or embryonic DNA was routinely genotyped by polymerase chain reaction (PCR) by using 30 cycles of 94°C for 20 s, 60°C for 30 s, and 72°C for 40 s, with the following primers: primer-1, 5′-GTCCACTTAGATCTGGTCTGTCTG-3′; primer-2, 5′-TAGAAACTCACCCTGTGAAGCGTC-3′; and primer-3, 5′-CAAACGGCGGATTGACCGTAATGG-3′.

Dissection of Embryos and Genotyping

Heterozygous mice were bred to obtain wild-type (*Tjp1*$^{+/+}$), heterozygote (*Tjp1*$^{+/-}$), and homozygous mutant (*Tjp1*$^{-/-}$) embryos. Mice were kept on a 12-h light-dark cycle, and the morning of the day on which a vaginal plug was detected was designated E0.5. Embryos were dissected from the uterus in phosphate-buffered saline (PBS), and dissected Reichert's membrane was used for genotyping. Reichert's membrane was digested for 6 h at 60°C in TP lysis buffer (50 mM Tris-Cl, pH 7.5, 0.1 M NaCl, 0.5% SDS, and 5 mM EDTA), containing 200 μg/ml proteinase K (Promega, Annandale, Australia) and boiled for 5 min before being subjected to PCR (as described above).

Immunoblotting

Protein was isolated from whole embryos in lysis buffer (62.5 mM Tris-Cl, pH 6.8, 2% glycerol, 1% SDS, 5 mM EDTA, and a protease inhibitor cocktail [Nakarai Tesque, Kyoto, Japan]), sonicated on ice five times for 3 s, and centrifuged at $48{,}000 \times g$ for 20 min at room temperature (RT). The supernatant (crude extract) was used for immunoblotting. Proteins separated by SDS-polyacrylamide gel electrophoresis on 10% acrylamide gels were electrophoretically transferred onto polyvinylidene difluoride membranes that were then incubated with the primary antibody. Bound antibodies were visualized with alkaline phosphatase-conjugated goat anti-rabbit and anti-mouse immunoglobulin G and the appropriate substrate as described by the manufacturer (GE Healthcare, Chalfont St. Giles, United Kingdom).

Histological Analysis

Embryos were isolated in PBS and photographed. For histological analyses, the embryos were fixed for 1 h in 4% paraformaldehyde (PFA) at RT, and then they were dehydrated and embedded in paraffin. Embryos were sectioned, and the sections were stained with hematoxylin and eosin.

Immunofluorescence Microscopy

Embryos were washed thoroughly with PBS, fixed for 30 min in PBS containing 4% PFA at RT, placed in a solution of 15% sucrose in PBS for 5 h, embedded in O.C.T. compound (Tissue-Tek, Sakura Finetek USA, Torrance, CA), and frozen using liquid nitrogen. Frozen sections, 6 μm in thickness, were cut on a cryostat, mounted on glass slides, air-dried, washed with PBS three times, and treated with 0.1% Triton X-100/PBS for 10 min. They were then processed for immunofluorescence microscopy as described previously (Adachi *et al*., 2006). Whole-mount embryos were immunostained for PECAM-1 to detect the vascular endothelium as described previously (Dominguez *et al*., 2007). For the analysis of immunofluorescence-labeled yolk sac whole mounts, yolk sacs were removed from the embryo after the fixing process, and they were stained as described previously (Umeda *et al*., 2004, 2006), and then they were attached to glass slides.

Isolation of RNA and Reverse Transcription (RT)-PCR

Total RNA was isolated from *Tjp1*$^{+/+}$ and *Tjp1*$^{-/-}$ yolk sac in E9.5 embryos, using an RNeasy microkit (QIAGEN, Valencia, CA). First-strand cDNAs were

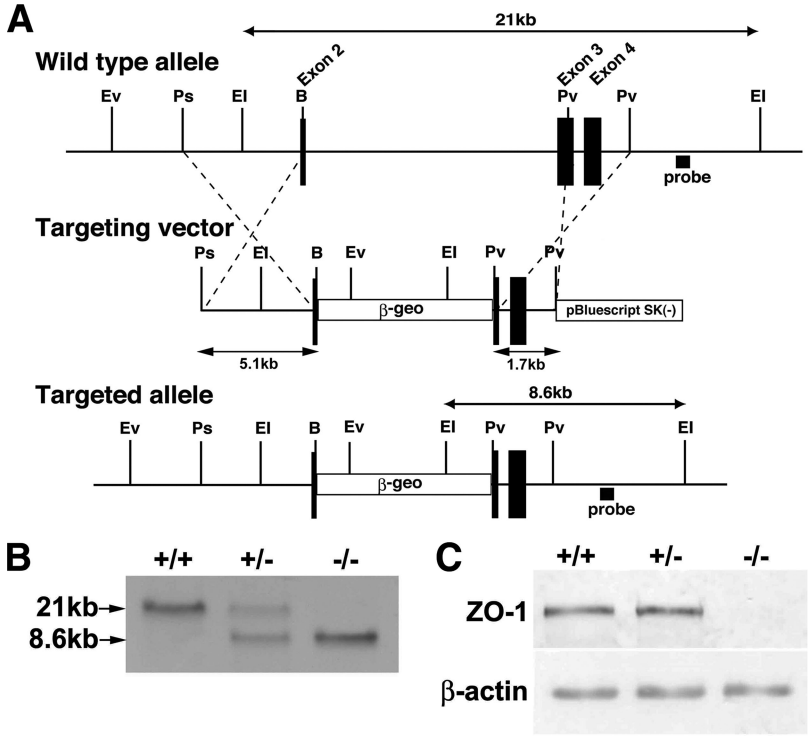

Figure 1. Generation of ZO-1–deficient mice. (A) Restriction maps of the wild type allele, the targeting vector, and the targeted allele of the ZO-1 gene. The targeting vector contained the pgk-neo cassette in its middle portion to delete the two to three exons in the targeted allele. The position of the probe for Southern blotting is indicated as a bar (Probe). Ev, EcoRV; Ps, PstI; EI, EcoRI; B, BsrDI; and Pv, PvuII. (B) Genotypic analysis by Southern blotting of EcoRI-digested genomic DNA from wild-type (+/+), heterozygous (+/−), and homozygous (−/−) mice for the ZO-1 gene allele. Southern blotting with the probe indicated in A yields 21- and 8-kb bands from the wild-type and targeted allele, respectively. (C) Loss of ZO-1 protein in the embryonic extract of $Tjp1^{-/-}$ mice examined by immunoblotting. Anti-ZO-1 immunoblotting of the embryonic protein extracts of ZO-1–deficient mice. Embryonic protein extracts (10 μg) from $Tjp1^{+/+}$ (+/+), $Tjp1^{+/-}$ (+/−), and $Tjp1^{-/-}$ (−/−) mice were immunoblotted with anti-ZO-1 mAb. In the wild-type and heterozygous embryonic extracts, the ZO-1 band is detected, whereas in the homozygous extract, this band is not detected.

generated, using SuperScript II reverse transcriptase, according to the manufacturer's directions (Invitrogen, Carlsbad, CA). The first-strand cDNAs (25 ng) were amplified by PCR using specific nucleotide primers. The primers for Tie-1 and Flt-1 were described previously (Baumer *et al*., 2006). The primers for PECAM-1, Flk-1, VE-cadherin, Tie-2, βH, and β-actin were also described previously (Gory-Faure *et al*., 1999). The primers for JAM-A were described previously (Cooke *et al*., 2006). The primers for ZO-1, ZO-2, and ZO-3 were with the following primers: ZO-1 primer-1, 5′-GCTAAGAGCACAGCAATGGA-3′; ZO-1 primer-2, 5′-GCATGTTCAACGTTATCCAT-3′; ZO-2 primer-1, 5′-CATGGGCGCGGACTATCT-3′; ZO-2 primer-2, 5′-CTGTGGCGGGGAGGTTTGA-3′; ZO-3 primer-1, 5′-CACGCAATCCTGGATGTCA-3′; and ZO-3 primer-2, 5′-GTCGCGCCTGCTGTTGCTGTA-3′. The amplification was performed using a step-down PCR as follows: three cycles: 94°C for 30 s, 69°C for 30 s, 72°C for 40 s; three cycles: 94°C for 30 s, 66°C for 30 s, 72°C for 40 s; three cycles: 94°C for 30 s, 63°C for 30 s, 72°C for 40 s; three cycles: 94°C for 30 s, 60°C for 30 s, 72°C for 40 s; and 25 cycles: 94°C for 30 s, 57°C for 30 s, 72°C for 40 s.

Barrier Assay

The biotin tracer assay was performed using the cell surface biotinylation method as described previously (Umeda *et al*., 2006), with some modifications. After the decidua and Reichert's membrane were carefully removed, embryos were washed with HEPES-buffered saline (HBS; 25 mM HEPES-NaOH, pH 7.2, 137 mM NaCl, 5 mM KCl, 0.7 mM Na_2HPO_4, 6 mM dextrose, and 1.8 mM $CaCl_2$). The endoderm of yolk sac was biotinylated by submerging the conceptus in HBS supplemented with 1 mg/ml EZ-Link Sulfo-NHS-LC-biotin (Pierce Chemical, Rockford, IL). The mesoderm of yolk sac and the embryo proper were biotinylated by injecting the same solution into the exocoelomic cavity using a mouth-held microcapillary pipette (Zeigler *et al*., 2006). After a 10-min incubation, embryos were washed with HBS, fixed with 4% formaldehyde in HBS for 10 min at RT, and processed for fluorescence microscopy with streptavidin-Texas Red (Calbiochem, San Diego, CA.).

RESULTS

Generation of $Tjp1^{-/-}$ Mice

To explore the function of ZO-1 in vivo, we attempted to homozygously disrupt the ZO-1 gene in mice. The genomic structure of the mouse ZO-1 gene was partially clarified. Exons 2–4 encoded most of the PDZ-1 domain. The targeting vector was constructed with the expectation that homologous recombination between the vectors and the ZO-1 gene would result in the deletion of a small portion of exon 2 and almost all of exon 3 (Figure 1A). The wild-type ZO-1 allele displayed a 21-kb band on Southern blotting of EcoRI-digest DNA with the 3′ probe, whereas the disrupted locus showed an 8.6-kb band (Figure 1B). To assess the impact of the mutant allele on ZO-1 protein levels, we performed Western blot analyses using an anti-ZO-1 mAb. ZO-1 protein was not detected in homozygous mutant ($Tjp1^{-/-}$) embryos (Figure 1C).

Embryonic Lethality Caused by Homozygous $Tjp1^{-/-}$ Mutation

$Tjp1^{+/-}$ mice were backcrossed with C57BL/6 wild-type mice through more than nine generations, and they were interbred to produce homozygous mice. Both male and female $Tjp1^{+/-}$ mice were allowed to grow for ~70 wk, and they showed no obvious phenotypes, with comparable fertility and growth rates to those of wild-type $Tjp1^{+/+}$ mice (data not shown). Intercrossing $Tjp1^{+/-}$ mice produced offspring, of which 36% were wild-type $Tjp1^{+/+}$ mice, 64% were heterozygous $Tjp1^{+/-}$ mice, and none were homozygous $Tjp1^{-/-}$ mice, thus leading us to examine the embryos. The examination of >200 embryos at various stages of gestation from ZO-1 heterozygous intercrosses revealed that $Tjp1^{-/-}$ embryos were indistinguishable from wild-type embryos up to E8.5. At E8.5, $Tjp1^{-/-}$ embryos were retarded, lagging at least 0.5 d behind the development of $Tjp1^{+/+}$ and $Tjp1^{+/-}$ littermates (Figure 2A). By E9.5 and E10.5, $Tjp1^{-/-}$ embryo proper displayed severe growth defects, most apparently, a significant reduction in size and an absence of turning (Figure 2, A and B). Furthermore, chorioallantoic fusion did not occur in the $Tjp1^{-/-}$ embryos (Figure 2, A and B). Defects were also apparent in the $Tjp1^{-/-}$ yolk sac extraembryonic region. Yolk sacs were not fully developed without normal patterning of vascularization in $Tjp1^{-/-}$ embryos, compared with wild-type $Tjp1^{+/+}$ litter embryos (Figure 2C). Together, defects in $Tjp1^{-/-}$ embryonic tissue were detected in embryonic and extraembryonic regions.

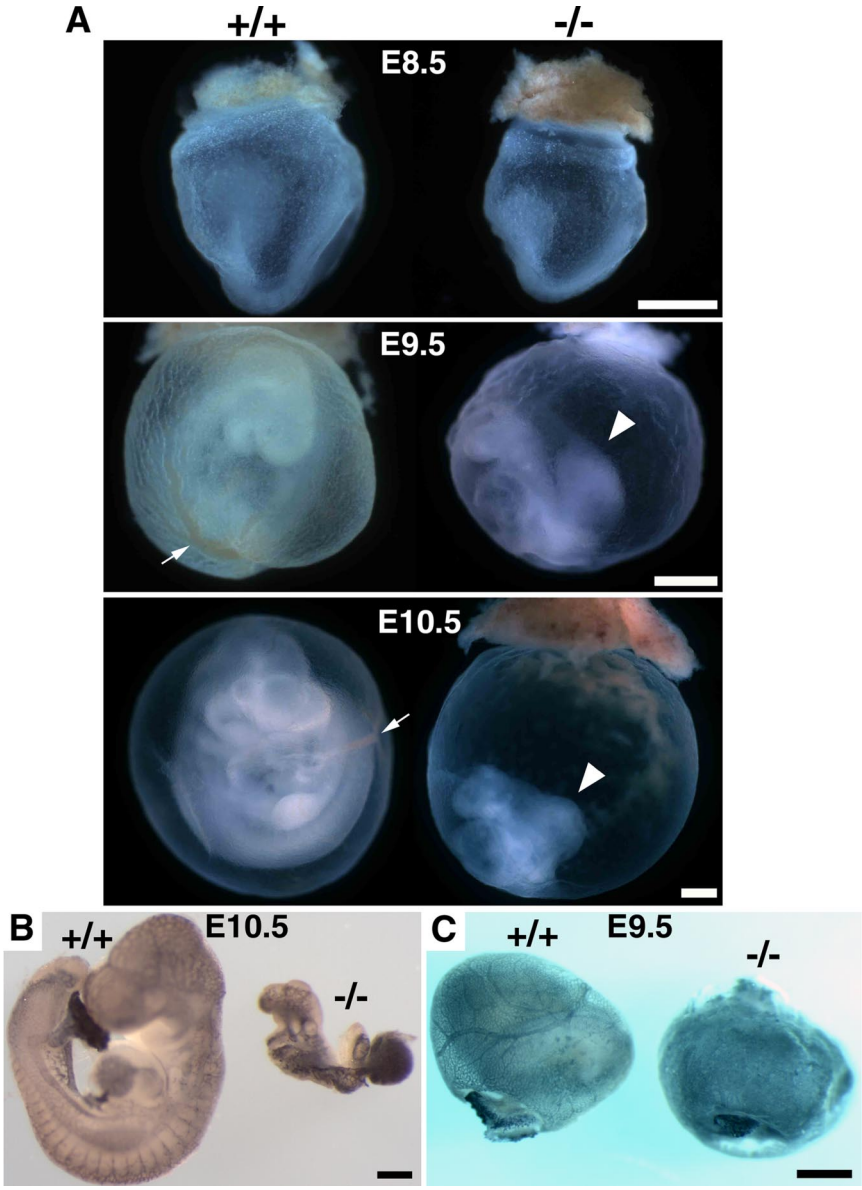

Figure 2. Macroscopic analysis of $Tjp1^{+/+}$ and $Tjp1^{-/-}$ embryos at E8.5-E10.5. (A) Photographs showing freshly dissected $Tjp1^{+/+}$ and $Tjp1^{-/-}$ embryos. Slight growth retardation was obvious in $Tjp1^{-/-}$ embryos compared with $Tjp1^{+/+}$ embryos at E8.5 (E8.5). From E9.5 onward, $Tjp1^{-/-}$ embryos were markedly smaller than $Tjp1^{+/+}$ embryos, and almost all failed to turn, a process that occurs in $Tjp1^{+/+}$ embryos around E9.0 (E9.5). Despite the obvious presence of an allantois (arrowhead) at E9.5 and E10.5, chorioallantoic fusion did not occur in the $Tjp1^{-/-}$ embryos. During E8.5 to E10.5, the $Tjp1^{-/-}$ embryo proper was approximately the same size, although the yolk sac was enlarged to a normal size, compared with $Tjp1^{+/+}$ litter embryos. The large vitelline vessels (arrows) were detected in $Tjp1^{+/+}$ yolk sac at E9.5 and E10.5. (B) PECAM-1 stained embryo proper. Although the growth was critically retarded, vasculogenesis, and angiogenesis occurred in the $Tjp1^{+/+}$ and $Tjp1^{-/-}$ embryo proper. (C) PECAM-1–stained embryonic yolk sac. Numerous large, branching vessels were present in $Tjp1^{+/+}$ yolk sacs as revealed by PECAM-1 staining, showing the process of angiogenesis. In contrast, the arrangement of branching vessels was not detected extraembryonically in $Tjp1^{-/-}$ yolk sacs, without signs of angiogenesis. Bars, 1 mm.

Although between E8.5 and E10.5 genotype ratios were consistent with the expected Mendelian distribution (Table 1), empty deciduas were detected at E11.5 and some $Tjp1^{-/-}$ embryos, present in litters, were partially resorbed and thus scored as nonviable. Between E11.5 and E12.5, several empty decidua were present, possibly due to the resorption of $Tjp1^{-/-}$ embryos at earlier stages of gestation, whereas $Tjp1^{+/+}$ and $Tjp1^{+/-}$ embryos remained in the same number as that before E10.5 with no $Tjp1^{-/-}$ embryos. These results strongly suggested that homozygosity for the ZO-1 null mutation induced embryonic death between E10.5 and E11.5 and that ZO-1 played an essential role in postimplantation in embryonic development.

Embryonic Defects in Growth and Turning Associated with Apoptosis in $Tjp1^{-/-}$ Mice

As revealed in hematoxylin- and eosin-stained sections of $Tjp1^{+/+}$ and $Tjp1^{-/-}$ E9.0 embryos (Figure 3), the posterior of $Tjp1^{+/+}$ and $Tjp1^{-/-}$ embryo proper showed the general organization of the neural tube, notochord, dorsal aorta, and hindgut in $Tjp1^{+/+}$ and $Tjp1^{-/-}$ E9.0 embryos. However, we detected hypertrophy of the notochord. Apoptotic or necrotic cells were detected in the notochord, neural tube, hindgut, and their surrounding mesenchym in $Tjp1^{-/-}$ em-

Table 1. Genotype analysis of offspring from $Tjp^{+/-}$ intercross

	No. of progeny			
Stage	+/+	+/−	−/−	Total
E8.5	16	29	15	60
E9.5	38	62	37	137
E10.5	16	26	13	55
E11.5	9	17	0 (12[a])	26
E12.5	5	14	0 (5[a])	19
Postnatal	79	140	0	219

[a] Resorbent.

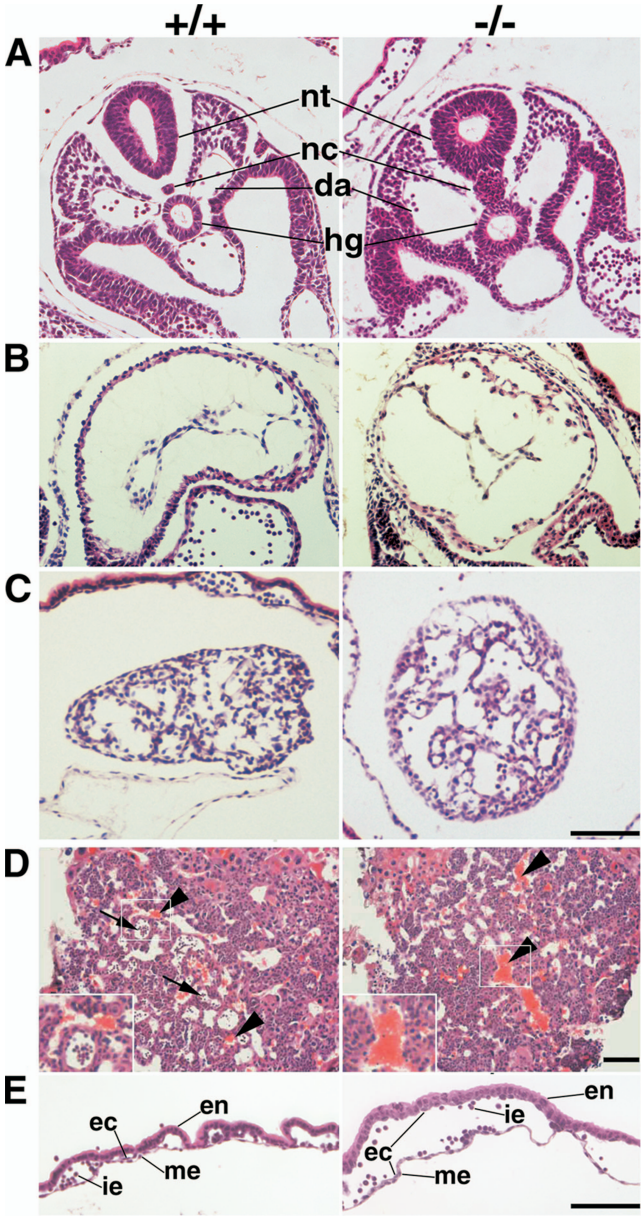

Figure 3. Histological analysis of transverse sections of *Tjp1*$^{+/+}$ and *Tjp1*$^{-/-}$ embryos at E9.0. (A) Caudal regions. The posterior of *Tjp1*$^{+/+}$ and *Tjp1*$^{-/-}$ embryos proper showed a normal neural tube (nt), dorsal aorta (da), and hindgut (hg), and an abnormal morphology of notochord (nc) in *Tjp1*$^{-/-}$ embryos. (B) Primitive heart. No obvious change was discerned between *Tjp1*$^{+/+}$ and *Tjp1*$^{-/-}$ embryos. (C) Allantois. Although *Tjp1*$^{-/-}$ allantois was associated with apoptosis, a well-defined vascular network was developed similar to the Tjp1$^{+/+}$ allantois. (D) Placentas. A transverse sectional analysis of *Tjp1*$^{+/+}$ placentas showed the presence of immature embryonic erythrocytes (arrows) and unnucleated maternal erythrocytes (arrowheads), whereas the labyrinth layer of *Tjp1*$^{-/-}$ embryos lacked immature embryonic nucleated erythrocytes and embryonic blood vessels derived from the mesoderm. Left bottom, high-magnification images of the boxed regions. (E) Yolk sac. In the *Tjp1*$^{+/+}$ yolk sac, the vessels were well formed, but in the *Tjp1*$^{-/-}$ yolk sac, the vessels were dramatically enlarged. Specific structures are as follows: en, extraembryonic endoderm; me, extraembryonic mesoderm; i.e., immature erythrocyte; and ec, endothelial cell. Bars, 100 μm.

bryos (Figures 3A and 4A). Although the deficiency of some adhesion molecules, such as N-cadherin, connexin-45, and α_4-integrin, induced defects in the morphogenesis of the heart (Yang *et al*., 1995; Radice *et al*., 1997; Kruger *et al*., 2000), no obvious change was observed in the primitive heart between *Tjp1*$^{+/+}$ and *Tjp1*$^{-/-}$ embryos (Figure 3B), with a spontaneous beating in the heart until E10.5.

Next, we examined whether the partial disorganization of the notochord and neural tube area was due to abnormal proliferation, apoptosis, or both. For this purpose, we immunofluorescently examined the proliferation and apoptosis in tangential sections of E8.5 and E9.5 embryos, by applying the proliferation marker Ki-67 and the apoptosis marker caspase-3, respectively. Although no clear difference in proliferation marker Ki-67 staining was detected, a significantly more intense staining for caspase-3 was detected in the notochord, neural tube, somite, and allantois in *Tjp1*$^{-/-}$ E9.5 embryos compared with *Tjp1*$^{+/+}$ E9.5 embryos (Figure 4, B and C). Thus, it was suggested that abnormal apoptosis occurred around E9.5, leading to the disorganization of the ventricular side of the neural tube, notochord, and other areas. Considering that ZO-1 is important in cell–cell adhesion, one possibility is that the embryonic defects were due to defects in highly organized ZO-1-based cell–cell adhesion.

Immunofluorescence Patterns for ZO-1, ZO-2, and ZO-3 in Embryos

Because ZO-1 was a member of the TJ-MAGUK family, we examined the respective localization of ZO-1, ZO-2, and ZO-3, in the *Tjp1*$^{+/+}$ embryos at E8.5 (Figure 5A). The signals for ZO-1 and ZO-2 were coexpressed in almost all types of cells at cell–cell contacts, except for the yolk sac extraembryonic mesoderm where the signal for ZO-1 but not for ZO-2 was detectable. ZO-3 was expressed in the outermost epithelial layer, and it was colocalized with ZO-1 and ZO-2. In *Tjp1*$^{-/-}$ embryos, the ZO-1-signal disappeared in the embryonic region without a compensatory increase in ZO-2/3 but with more strict concentration of ZO-2 into TJs; and in Western blot analysis, there were no differences in protein expression of ZO-2/3 between *Tjp1*$^{+/+}$ *and Tjp*$^{-/-}$ embryos (Supplemental Figure 2).

Extraembryonic Defects in Tjp1$^{-/-}$ *Mice*

Extraembryonic development and differentiation are critical for normal embryonic proper development and differentiation. Although there is no substantial changes in the morphology between *Tjp1*$^{+/+}$ and *Tjp1*$^{-/-}$ embryos, *Tjp1*$^{--}$ embryos underwent apoptic or necrotic cells in allantois (Figure 3C), as revealed in hematoxylin- and eosin-stained sections of allantois, which was abnormally a large, swollen sac and not fused with the chorion in *Tjp1*$^{-/-}$ embryos (Figure 2A). In placenta, the labyrinth layer of *Tjp1*$^{-/-}$ embryos lacked immature embryonic nucleated erythrocytes and embryonic blood vessels derived from the mesoderm (Figure 3D), possibly due to the lack of chorionic fusion. The defined vessel formation was seen in *Tjp1*$^{+/+}$ yolk sacs, but not detected in *Tjp1*$^{-/-}$ yolk sacs. The *Tjp1*$^{-/-}$ extraembryonic endoderm and mesoderm layers were more widely separated than *Tjp1*$^{+/+}$ layers with no apoptotic cells (Figure 3E). In immunolabeling analysis of sections of yolk sac, it was noteworthy that only ZO-1 was detected in the extraembryonic mesoderm without ZO-2/3 and that in *Tjp1*$^{-/-}$ embryos, the extraembryonic mesoderm lacked ZO1/2/3 (Figure 5B).

Defects in Angiogenesis in Tjp1$^{-/-}$ *Embryos*

The preformed primitive vascular plexus begins to be remodeled in the yolk sacs of *Tjp1*$^{+/+}$ embryos by E8.5, so that the yolk sacs have an organized vascular network of branching vessels at E9.5, which are lined with PECAM-1–positive endo-

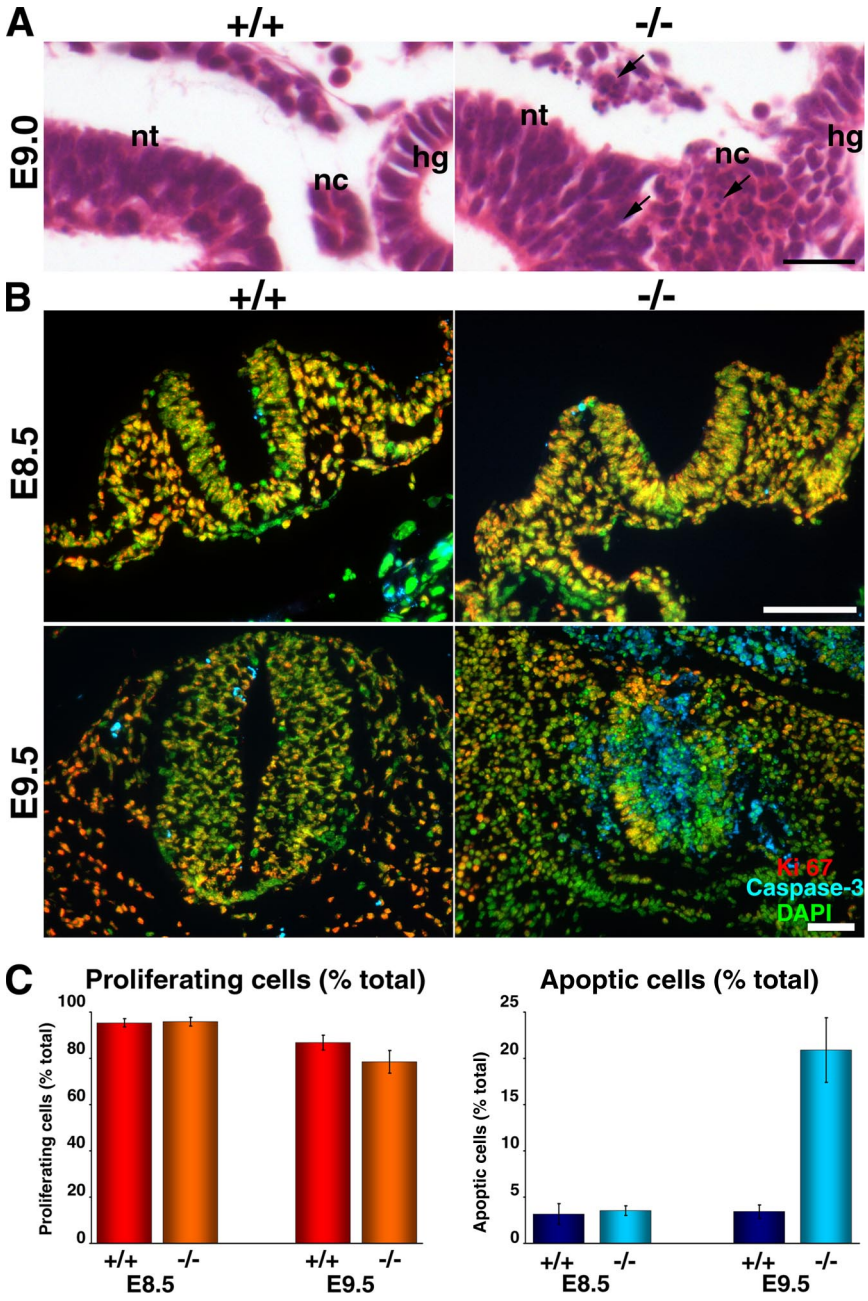

Figure 4. Apoptosis in $Tjp1^{+/+}$ and $Tjp1^{-/-}$ embryos at E8.5 to E9.5. (A) Hematoxylin- and eosin-stained transverse sectional images of embryos at E9.0 around the notochord. In $Tjp1^{-/-}$ embryos, the border of the notochord (nc) seemed to be disorganized. $Tjp1^{-/-}$ embryos showed the presence of apoptotic or necrotic cells (arrows) at the notochord, neural tube, hindgut, and mesenchym around them. Specific structures are as follows: nt, neural tube; hg, hind gut; and nc, notochord. Bar, 20 μm. (B) Immunofluorescence images for Ki-67, caspase-3, and DAPI. At E8.5, almost no changes were detected between $Tjp1^{+/+}$ and $Tjp1^{-/-}$ embryos. At E9.5, in $Tjp1^{-/-}$ embryos, caspase-3–positive apoptotic cells scattered beyond the normal bordered layer of the notochord or neural tube, whereas little apoptotic cells were detected in litter $Tjp1^{+/+}$ embryos. (C) Quantification of Ki-67 and caspase-3–positive cells (mean and SE [n = 6]). Caspase-3 signals suggested that in $Tjp1^{-/-}$ embryos, the apoptotic cells were significantly increased compared with $Tjp1^{+/+}$ embryos. Bars, 50 μm.

thelial cells. Although the initial primitive vascular plexus was formed in $Tjp1^{-/-}$ yolk sacs at E8.5, PECAM-1 immunostaining confirmed the lack of any identifiable mature or remodeled blood vessels in $Tjp1^{-/-}$ yolk sacs around E9.5 (Figure 6A). In contrast to the compartmentalization that was developed in $Tjp1^{+/+}$ embryos, these $Tjp1^{-/-}$ vessels continued to expand without compartments, except for very few remaining adhesion sites, as shown in the cross-sectional images. Even with these severe morphological defects, the endothelial cell layers themselves seem normal in the extraembryonic endoderm and mesoderm in $Tjp1^{-/-}$ embryos (Figure 3E). When the expression of endothelial markers and hematopoietic markers was analyzed by RT-PCR using E9.5 $Tjp1^{+/+}$ and $Tjp1^{-/-}$ yolk sacs (Supplemental Figure 2), it was revealed that in $Tjp1^{-/-}$ yolk sacs, all markers were expressed normally, in the same way as those in $Tjp1^{+/+}$ yolk sacs. In contrast to PECAM-1 and VE-cadherin, which showed the same localization in cell–cell adhesion sites between $Tjp1^{+/+}$ and $Tjp1^{-/-}$ yolk sacs, JAM-A was localized in the cell–cell adhesion sites of $Tjp1^{+/+}$ yolk sacs, but it was not localized there in $Tjp1^{-/-}$ yolk sacs (Figure 6B). These results suggested that vasculogenesis occurred normally in $Tjp^{-/-}$ yolk sacs, whereas angiogenesis was abnormal, compared with $Tjp1^{+/+}$yolk sacs, possibly due to some defects in cell–cell adhesion-related tissue remodeling.

Barrier Assay in Tjp$^{-/-}$ Extraembryonic Regions

Because severe morphological defects were recognized in angiogenesis in $Tjp1^{-/-}$ embryos, we examined the barrier function of vessels in $Tjp1^{-/-}$ embryos compared with $Tjp1^{+/+}$ embryos. When a biotinylation reagent was applied from the outside of the $Tjp1^{+/+}$ and $Tjp1^{-/-}$ yolk sac, no infiltration was observed (Figure 7A). In contrast, when it was subcutaneously

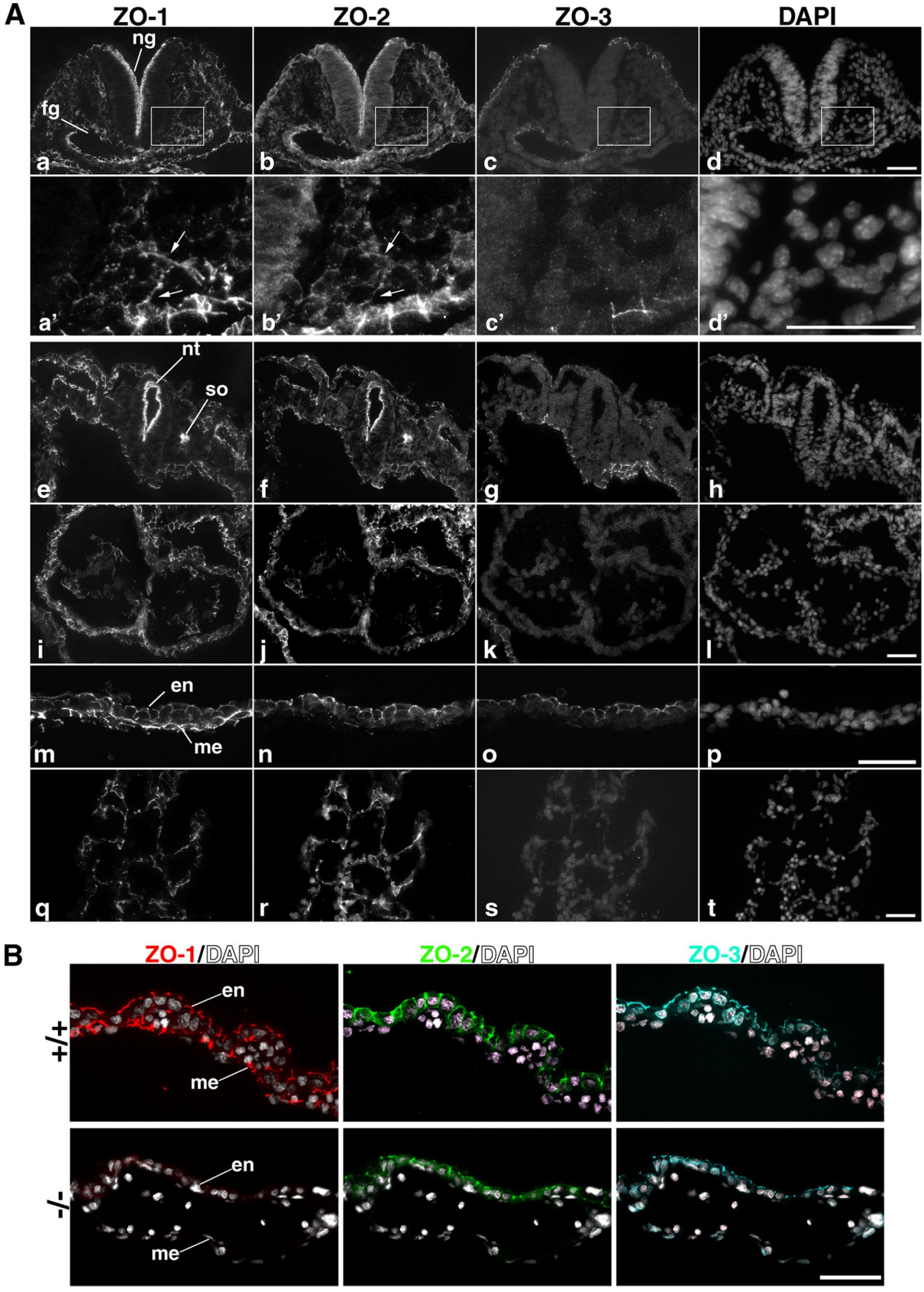

Figure 5. Immunolabeling of ZO-1, ZO-2, and ZO-3 in E8.5 wild-type *Tjp1*$^{+/+}$ embryos. (A) a–d, caudal parts of embryos. a′-d′, high magnification of the boxed region of caudal parts of embryos, each corresponding to a–d, respectively. ZO-1 and ZO-2 localized at cell–cell junctions in the mesenchymal cells (arrows). e–h, cephalic parts of embryos. i–l, primitive heart. m–p, yolk sac. q–t, allantois. Specific

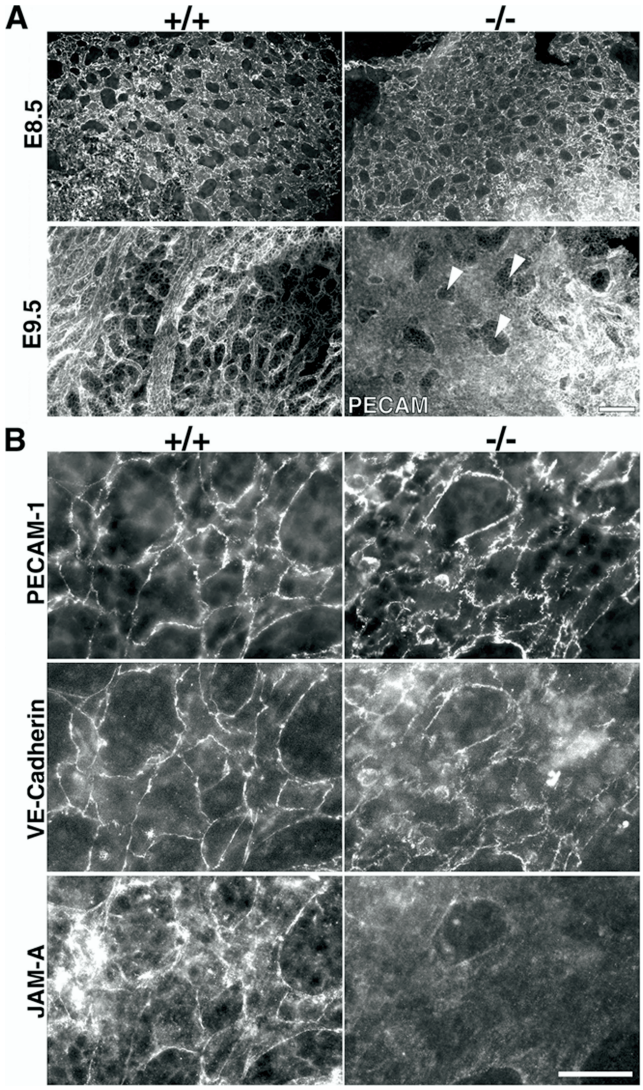

Figure 6. Analysis of yolk sac extraembryonic vascular development. (A) Immunolabeling for PECAM-1 in whole-mount yolk sacs of E8.5 and E9.5 embryos of $Tjp1^{+/+}$ and $Tjp1^{-/-}$ mice. The immunostaining revealed whole patterns of vasculate not differing between $Tjp1^{+/+}$ and $Tjp1^{-/-}$ embryos at E8.5, although at E9.5, PECAM-1–stained vasculates were quite different. $Tjp1^{-/-}$ extraembryonic mesoderm lacked the fine branched arrangements of vessels constituted by angiogenesis. The connection sites between extraembryonic endoderm and mesoderm were indicated by arrowheads. (B) High-resolution immunofluorescence micrographs labeled for PECAM-1, VE-cadherin, and JAM-A. It was noted that the immunofluorescently labeled patterns for JAM-A, but not for PECAM-1 and VE-cadherin, differed between E8.5 $Tjp1^{+/+}$ and $Tjp1^{-/-}$ yolk sac. Bars, 100 μm (A) and 25 μm (B).

Figure 5 (cont). structures are as follows: ng, neural groove; fg, foregut; nt, neural tube; so, somite; en, extraembryonic endoderm; and me, extraembryonic mesoderm. Bars, 50 μm (a–d and e–t), 20 μm (a′–d′). (B) Immunofluorescence images of frozen sections of $Tjp1^{+/+}$ and $Tjp1^{-/-}$ yolk sacs at E9.5 stained for ZO-1, ZO-2, and ZO-3, respectively. In the wild-type $Tjp1^{+/+}$ yolk sac, ZO-1 was expressed in the extraembryonic endoderm and mesoderm, whereas in the homozygous $Tjp1^{-/-}$ yolk sac, signals for ZO-1 became undetectable. ZO-2 and ZO-3 were expressed only in extraembryonic endoderm in $Tjp1^{+/+}$ embryos. Note that the ZO-2 signal was apically concentrated in the $Tjp1^{-/-}$ extraembryonic endoderm. Specific structures are as follows: en, extraembryonic endoderm; and me, extraembryonic mesoderm. Bars, 50 μm.

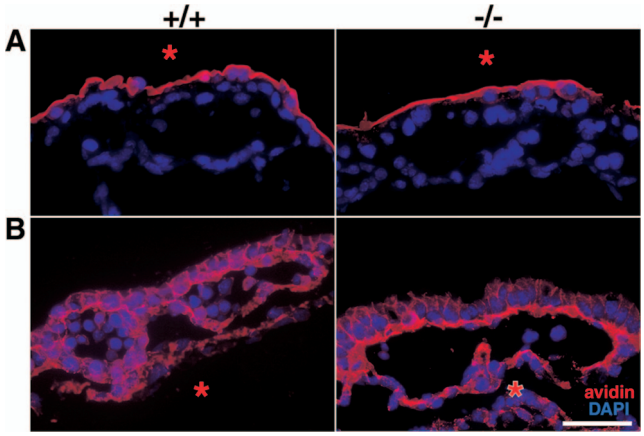

Figure 7. Paracellular barrier assay of the $Tjp1^{+/+}$ and $Tjp1^{-/-}$ yolk sac at E9.5. (A) Biotinylation from the outside of yolk sacs in $Tjp1^{+/+}$ and $Tjp1^{-/-}$ embryos. Conjugated biotin was detected with avidin-Texas Red, which did not penetrate the paracellular barrier. (B) Biotinylation from the inside of yolk sac in $Tjp1^{+/+}$ and $Tjp1^{-/-}$ embryos. When biotin was subcutaneously injected into the excoelomic cavity (*), it was spread beyond the extraembryonic mesodermal cell sheets, showing no barrier function in the extraembryonic mesoderm. Bar, 50 μm.

injected into the excoelomic cavity of E9.5 $Tjp1^{+/+}$ and $Tjp1^{-/-}$ yolk sac, the reagent passed through the $Tjp1^{+/+}$ and $Tjp1^{-/-}$ yolk sacs to the most apical cell–cell contacts (Figure 7B). These results indicated that extraembryonic yolk sac endodermal cell sheets were typical epithelial cell sheets, functioning as a barrier for biotin, and that the yolk sac extraembryonic mesodermal cell sheets did not strictly act as a barrier, although linear ZO-1 staining was observed.

Whole-Mount Immunofluorescence Staining for ZO-1, ZO-2, and ZO-3 in York Sac Endoderm and Mesoderm

Previously, we generated ZO-1(KO)/ZO-2(KD) epithelial Eph4 cultured cells that did not express ZO-3 genetically. Thus, the ZO-1(KO)/ZO-2(KD) epithelial Eph4 cells had no ZO-1/2/3, in which the formation of AJs was abnormal without formation of TJs (Umeda *et al*., 2006; Ikenouchi *et al*., 2007). Because the yolk sac extraembryonic mesoderm lacked ZO-1/2/3 in $Tjp1^{-/-}$ embryos, we examined the morphology of the developing sheets of the yolk sac in detail by whole-mount immunostaining for cell–cell adhesion-related molecules (Figure 8). The immunofluorescence pattern of ZO-1/2/3 in $Tjp1^{+/+}$ embryos showed a fine linear pattern, typical of TJs, suggesting that these TJ-MAGUK proteins were associated with TJs, although ZO-2 seemed to be more broadly distributed around TJs, not only just on TJs. The clear line stained for the TJ-MAGUK proteins was positive for claudins, occludin, or both, except for yolk sac extraembryonic mesoderm which were positive for ZO-1 but negative for other TJs-related proteins (ZO-2/3, occludin, claudin-6, JAM-A, and cingulin) (Figure 8). In contrast, in the yolk sac $Tjp1^{-/-}$ extraembryonic regions, the immunofluorescence patterns of ZO-2 were slightly changed from a somewhat broad pattern around TJs to a sharper pattern, compared with those of $Tjp1^{+/+}$ extraembryonic regions, suggesting some functionally redundant role of ZO-2 for ZO-1. In $Tjp1^{-/-}$ yolk sac, the extraembryonic endodermal and mesodermal cell sheet layer was normally formed, suggesting a normal vasculogenesis.

DISCUSSION

The embryonic lethal phenotype of $Tjp1^{-/-}$ mice has revealed the essential role of ZO-1. Embryonic and extraem-

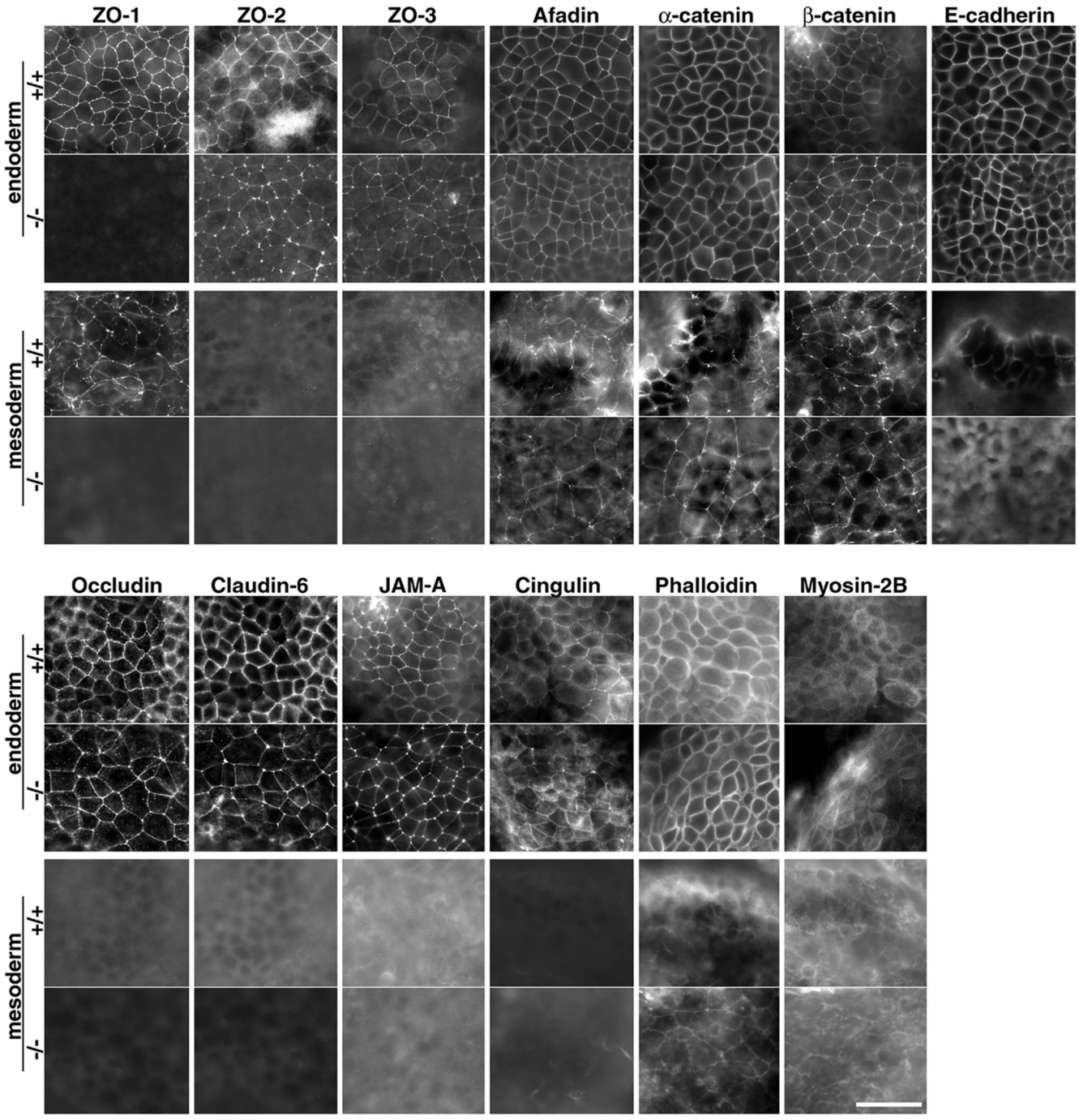

Figure 8. Whole-mount immunofluorescence micrographs of extraembryonic endoderm and mesoderm for cell–cell adhesion-related proteins in *Tjp1*$^{+/+}$ and *Tjp1*$^{-/-}$ mice at E 9.5. In *Tjp1*$^{+/+}$ and *Tjp1*$^{-/-}$ extraembryonic endoderm, the immunofluorescence patterns for various types of cell adhesion-related proteins revealed the normal formation of the epithelial cell sheets with TJs. It is noteworthy that the ZO-2 signal was concentrated in cell–cell adhesion sites of the *Tjp1*$^{-/-}$ extraembryonic endoderm. Furthermore, the immunofluorescence patterns of TJ-related proteins such as occludin, claudin-6, and JAM-A were also concentrated in cell–cell adhesion sites of the *Tjp1*$^{-/-}$ extraembryonic endoderm. In contrast, in extraembryonic mesoderm, the immunofluorescence patterns of afadin and α/β-catenin substantiated cell sheet formation but without concentration of TJ-proper proteins, such as occludin, claudin, and JAM-A. Note that in *ZO-1*$^{-/-}$ extraembryonic mesoderm, the signals for ZO-1/2/3 were not detected. Bar, 50 μm.

bryonic defects were both recognized around E9.5. It is possible that the extraembryonic defects in yolk sac angiogenesis and allantois fusion associated with apoptosis were the most primary ones. Conversely, it is also possible that embryonic defects based on a ZO-1 deficiency caused embryonic lethality associated with apoptosis in the notochord, neural tube, hindgut, and somite. Recent biochemical studies of the TJ-MAGUK family have revealed that ZO-1 and ZO-2 share properties such as claudin binding and α-catenin binding, with their different molecular weights mainly related to the different number of amino acids in actin binding domains (Mitic and Anderson, 1998; Gonzalez-Mariscal *et*

al., 2000). The cell level analysis showed that a large part of the ZO-1 knockout/ZO-2 knockdown phenotypes were similarly rescued by either ZO-1 or ZO-2; however, in ZO-1-deficient epithelial Eph4 cells, overexpression of ZO-2 does not rescue the delayed formation of TJs (Umeda *et al*., 2004). In a reasonably consistent way, it was recently reported that ZO-2–deficient *Tjp2*$^{-/-}$ mice, compared with wild-type embryos, died shortly after implantation because of arrest in early gastrulation with increased apoptosis at E7.5 (Xu *et al*., 2008). Thus, ZO-1 and ZO-2 were not redundant in the early development of embryos. It is reported that ZO-3 plays a role distinct from that of ZO-1/2 and that ZO-3 deficiency produces no phenotypes at cellular and mouse levels (Umeda *et al*., 2004, 2006; Adachi *et al*., 2006; Xu *et al*., 2008). Hence, the mouse level analysis revealed that the closely related proteins, ZO-1/2/3 were not redundant to each other.

In ZO-2–deficient mice, some defects were recognized in the function of the junctional complex, the paracellular barrier function, and also in the tissue organization caused by apoptosis. These might possibly rationalize the earlier timing of lethality of *Tjp2*$^{-/-}$ mice compared with *Tjp1*$^{-/-}$ mice, in which defects in the junctional function itself were not detected. The present study showed that the expression patterns of ZO-1 and ZO-2 were basically very similar in wild-type *Tjp1*$^{+/+}$ embryos, except in the yolk sac extraembryonic mesoderm in which ZO-1, but not ZO-2 or ZO-3, was expressed. Hence, no ZO-1/2/3 were expressed in the yolk sac extraembryonic mesoderm in *Tjp1*$^{-/-}$ embryos, in which we could detect the mislocalization of JAM-A, a component of TJs as well as AJs, and defects in angiogenesis compared with *Tjp1*$^{+/+}$ mice. Thus, these findings suggested a role for ZO-1/2 in determining cell fate and remodeling in a cell adhesion-related way.

Although the connection of yolk sac mesodermal and endodermal layers, an important angiogenesis process (Drake and Little, 1995; Djonov *et al*., 2003; Coultas *et al*., 2005), was significantly inhibited by a deficiency of ZO-1, it remains unclear how the absence of ZO-1 and the mislocalization of JAM-A were related with defective angiogenesis in *Tjp1*$^{-/-}$ embryos. It is possible that ZO-1, JAM-A, or both played an important role in the remodeling for connection between the yolk sac mesoderm and endoderm layers in angiogenesis by directly or indirectly organizing some aspects of cell–cell adhesion in such a way that its deficiency inhibited angiogenesis. In this respect, it is reported that fibroblast growth factor-2–induced angiogenesis is defective in the JAM-A–deficient mice (Cooke *et al*., 2006). We could not recognize other abnormal patterns of TJ components in *Tjp1*$^{-/-}$ mouse epithelia, except for more concentrated ZO-2 staining in junctional patterns compared with *Tjp1*$^{+/+}$ epithelia, suggesting a partial redundant role of ZO-2 in place of ZO-1 in *Tjp1*$^{-/-}$ embryo and extraembryonic regions. However, the embryonic lethal phenotypes of ZO-1- and ZO-2–deficient mice contradicted any redundancy.

In parallel with the possibility that the embryonic hypertrophy was indirectly induced by the defects in extraembryonic angiogenesis, it is also possible that because of some defects related to ZO-1 deficiency in cell remodeling in *Tjp1*$^{-/-}$ embryos in the notochord, neural tube, hindgut and surrounding mesenchyme, the cells in these regions were directly lead to apoptosis. The restriction of the apoptotic area contrasted to the case of Edd- and connexin-45–deficient mice in which apoptosis occurred almost everywhere in embryos (at E9.5) indirectly caused by extraembryonic defects in angiogenesis. As well, reports on similar phenotypes (Goh *et al*., 1997; Radice *et al*., 1997; Kruger *et al*., 2000; Saunders *et al*., 2004; Argraves and Drake, 2005; Baumer *et al*., 2006; Morin-Kensicki *et al*., 2006; Dominguez *et al*., 2007) might possibly provide some clues about the mechanistic bases for the phenotypes in *Tjp1*$^{-/-}$ mice. In the *Drosophila* tracheal system, the *Drosophila* homologue of ZO-1, Polychaetoid, is suggested to be involved in AJ remodeling in epithelial morphogenesis, partially consistent with our findings in embryonic and extraembryonic regions (Jung *et al*., 2006). Thus, it is possible that apoptosis was induced in the specific embryonic region most possibly because of defects in cell modeling in *Tjp1*$^{-/-}$ mice.

Accumulated cases report that defects in the visceral yolk sac and allantois lead to retarded growth of the embryo and early lethality because of defective blood circulation (Radice *et al*., 1997; Kruger *et al*., 2000; Rossant and Cross, 2001; Copp, 1995; Saunders *et al*., 2004); both of which were defective features in *Tjp1*$^{-/-}$ embryos. It is noteworthy that the phenotypically related factors were VCAM-1, α_4-, α_5-integrin, connexin-45, VE-cadherin, and N-cadherin, which were possibly related to cell–cell interactions (Kwee *et al*., 1995; Yang *et al*., 1995; Goh *et al*., 1997; Radice *et al*., 1997; Gory-Faure *et al*., 1999; Kruger *et al*., 2000). In this regard, the secondary effects of extraembryonic defects on embryonic defects could be critically tested by using tetraploid rescue (Mackay and West, 2005) or through the generation of conditional knockout animals in which ZO-1 expression is disrupted only in embryonic tissue. These remain as future issues. As well, a sophisticated assay system seems needed for better functional analysis of ZO-1 in embryogenesis. The establishment of culture systems from *Tpj1*$^{-/-}$ mice provides a novel way to understand the function of TJ-MAGUK family members and to establish possible therapeutic strategies for related diseases. Studies are presently being conducted along these lines in our laboratory.

ACKNOWLEDGMENTS

We thank Tsutomu Otani (Department of Pathology and Tumor Biology, Graduate School of Medicine, Kyoto University, Kyoto, Japan) for excellent technical assistance in histologic analysis. We are grateful to Junichi Ikenouchi (Researcher, Japan Science and Technology Agency), Hisashi Nojima, Yuji Yamazaki, Tomoki Yano, and all laboratory members (Laboratory of Biological Science, Graduate School of Frontier Biosciences and Graduate School of Medicine, Osaka University) and Creative Scientific Research for production of anti-afadin antibodies and for participation in helpful and enlightening discussions. This study was supported by a grant-in-aid for Cancer Research from the Ministry of Education, Culture, Sports, Science and Technology of Japan, and Solution Oriented Research for Science and Technology, Japan Science and Technology Corporation (to Sa.T. and Sh.T.).

REFERENCES

Adachi, M., Inoko, A., Hata, M., Furuse, K., Umeda, K., Itoh, M., and Tsukita, Sh. (2006). Normal establishment of epithelial tight junctions in mice and cultured cells lacking expression of ZO-3, a tight-Junction MAGUK Protein. Mol. Cell Biol. *26*, 9003–9015.

Argraves, W. S., and Drake, C. J. (2005). Genes critical to vasculogenesis as defined by systematic analysis of vascular defects in knockout mice. Anat. Rec. A Discov. Mol. Cell Evol. Biol. *286*, 875–884.

Balda, M. S., Gonzalez-Mariscal, L., Matter, K., Cereijido, M., and Anderson, J. M. (1993). Assembly of the tight junction: the role of diacylglycerol. J. Cell Biol. *123*, 293–302.

Baumer, S., Keller, L., Holtmann, A., Funke, R., August, B., Gamp, A., Wolburg, H., Wolburg-Buchholz, K., Deutsch, U., and Vestweber, D. (2006). Vascular endothelial cell–specific phosphotyrosine phosphatase (VE-PTP) activity is required for blood vessel development. Blood *107*, 4754–4762.

Bazzoni, G., Martinez-Estrada, O. M., Orsenigo, F., Cordenonsi, M., Citi, S., and Dejana, E. (2000). Interaction of junctional adhesion molecule with the tight junction components ZO-1, cingulin, and occludin. J. Biol. Chem. *275*, 20520–20526.

Carmeliet, P. *et al*. (1997). Insights in vessel development and vascular disorders using targeted inactivation and transfer of vascular endothelial growth factor, the tissue factor receptor, and the plasminogen system. Ann. N Y Acad. Sci. *811*, 191–206.

Cooke, V. G., Naik, M. U., and Naik, U. P. (2006). Fibroblast growth factor-2 failed to induce angiogenesis in junctional adhesion molecule-A-deficient mice. Arterioscler. Thromb. Vasc. Biol. *26*, 2005–2011.

Copp, A. J. (1995). Death before birth: clues from gene knockouts and mutations. Trends Genet. *11*, 87–93.

Coultas, L., Chawengsaksophak, K., and Rossant, J. (2005). Endothelial cells and VEGF in vascular development. Nature *438*, 937–945.

Djonov, V., Baum, O., and Burri, P. H. (2003). Vascular remodeling by intussusceptive angiogenesis. Cell Tissue Res. *314*, 107–117.

Dominguez, M. G. *et al*. (2007). Vascular endothelial tyrosine phosphatase (VE-PTP)-null mice undergo vasculogenesis but die embryonically because of defects in angiogenesis. Proc. Natl. Acad. Sci. USA *104*, 3243–3248.

Drake, C. J., and Little, C. D. (1995). Exogenous vascular endothelial growth factor induces malformed and hyperfused vessels during embryonic neovascularization. Proc. Natl. Acad. Sci. USA *92*, 7657–7661.

Fanning, A. S., Jameson, B. J., Jesaitis, L. A., and Anderson, J. M. (1998). The tight junction protein ZO-1 establishes a link between the transmembrane protein occludin and the actin cytoskeleton. J. Biol. Chem. *273*, 29745–29753.

Furuse, M., Itoh, M., Hirase, T., Nagafuchi, A., Yonemura, S., Tsukita, Sa., and Tsukita, Sh. (1994). Direct association of occludin with ZO-1 and its possible involvement in the localization of occludin at tight junctions. J. Cell Biol. *127*, 1617–1626.

Goh, K. L., Yang, J. T., and Hynes, R. O. (1997). Mesodermal defects and cranial neural crest apoptosis in alpha5 integrin-null embryos. Development *124*, 4309–4319.

Gonzalez-Mariscal, L., Betanzos, A., and Avila-Flores, A. (2000). MAGUK proteins: structure and role in the tight junction. Semin. Cell Dev. Biol. *11*, 315–324.

Gory-Faure, S., Prandini, M. H., Pointu, H., Roullot, V., Pignot-Paintrand, I., Vernet, M., and Huber, P. (1999). Role of vascular endothelial-cadherin in vascular morphogenesis. Development *126*, 2093–2102.

Gumbiner, B., Lowenkopf, T., and Apatira, D. (1999). Identification of a 160-kDa Polypeptide that Binds to the Tight Junction Protein ZO-1. Proc. Natl. Acad. Sci. USA *88*, 3460–3464.

Halbleib, J. M., and Nelson, W. J. (2006). Cadherins in development: cell adhesion, sorting, and tissue morphogenesis. Genes Dev. *20*, 3199–3214.

Haskins, J., Gu, L., Wittchen, E. S., Hibbard, J., and Stevenson, B. R. (1998). ZO-3, a novel member of the MAGUK protein family found at the tight junction, interacts with ZO-1 and occludin. J. Cell Biol. *141*, 199–208.

Hernandez, S., Chavez-Munguia, B., and Gonzalez-Mariscal, L. (2007). ZO-2 silencing in epithelial cells perturbs the gate and fence function of tight junctions and leads to an atypical monolayer architecture. Exp. Cell Res. *313*, 1533–1547.

Ikenouchi, J., Umeda, K., Tsukita, Sa., Furuse, M., and Tsukita, Sh. (2007). Requirement of ZO-1 for the formation of belt-like adherens junctions during epithelial cell polarization. J. Cell Biol. *176*, 779–786.

Inoko, A., Itoh, M., Tamura, A., Matsuda, M., Furuse, M., and Tsukita. S. (2003). Expression and distribution of ZO-3, a tight junction MAGUK protein, in mouse tissues. Genes Cells *8*, 837–845.

Itoh, M., Furuse, M., Morita, K., Kubota, K., Saitou, M., and Tsukita, Sh. (1999). Direct binding of three tight junction-associated MAGUKs, ZO-1, ZO-2, and ZO-3, with the COOH termini of claudins. J. Cell Biol. *147*, 1351–1363.

Itoh, M., Nagafuchi, A., Moroi, S., and Tsukita, Sh. (1997). Involvement of ZO-1 in cadherin-based cell adhesion through its direct binding to α-catenin and actin filaments. J. Cell Biol. *138*, 181–192.

Itoh, M., Nagafuchi, A., Yonemura, S., Kitani-Yasuda, T., Tsukita, Sa., and Tsukita, Sh. (1993). The 220-kD protein colocalizing with cadherins in non-epithelial cells is identical to ZO-1, a tight junction-associated protein in epithelial cells: cDNA cloning and immunoelectron microscopy. J. Cell Biol. *121*, 491–502.

Jesaitis, L. A., and Goodenough, D. A. (1996). The tight junction protein ZO-2 contains three PDZ (PSD-95/Discs-Large/ZO-1) domains and an alternatively spliced region. J. Biol. Chem. *271*, 25723–25726.

Jung, A. C., Ribeiro, C., Michaut, L., Certa, U., and Affolter, M. (2006). Polychaetoid/ZO-1 is required for cell specification and rearrangement during *Drosophila* tracheal morphogenesis. Curr. Biol. *16*, 1224–1231.

Kitajiri, S. *et al*. (2004). Compartmentalization established by claudin-11-based tight junctions in stria vascularis is required for hearing through generation of endocochlear potential. J. Cell Sci. *117*, 5087–5096.

Komiya, S., Shimizu, M., Ikenouchi, J., Yonemura, S., Matsui, T., Fukunaga, Y., Liu, H., Endo, F., Tsukita, Sh., and Nagafuchi, A. (2005). Apical membrane and junctional complex formation during simple epithelial cell differentiation of F9 cells. Genes Cells *10*, 1065–1080.

Kruger, O., Plum, A., Kim, J. S., Winterhager, E., Maxeiner, S., Hallas, G., Kirchhoff, S., Traub, O., Lamers, W. H., and Willecke, K. (2000). Defective vascular development in connexin 45-deficient mice. Development *127*, 4179–4193.

Kwee, L., Baldwin, H. S., Shen, H. M., Stewart, C. L., Buck, C., Buck, C. A., and Labow, M. A. (1995). Defective development of the embryonic and extraembryonic circulatory systems in vascular cell adhesion molecule (VCAM-1) deficient mice. Development *121*, 489–503.

Mackay, G. E., and West, J. D. (2005). Fate of tetraploid cells in 4n↔ 2n chimeric mouse blastocysts. Mech. Dev. *122*, 1266–1281.

Mitic, L. L., and Anderson, J. M. (1998). Molecular architecture of tight junctions. Annu. Rev. Physiol. *60*, 121–142.

Morin-Kensicki, E. M., Boone, B. N., Howell, M., Stonebraker, J. R., Teed, J., Alb, J. G., Magnuson, T. R., O'Neal, W., and Milgram, S. L. (2006). Defects in yolk sac vasculogenesis, chorioallantoic fusion, and embryonic axis elongation in mice with targeted disruption of Yap65. Mol. Cell Biol. *26*, 77–87.

Morita, K., Sasaki, H., Furuse, M., and Tsukita, Sh. (1999). Endothelial claudin: claudin-5/TMVCF constitutes tight junction strands in endothelial cells. J. Cell Biol. *147*, 185–194.

Ohnishi, H., Nakahara, T., Furuse, K., Sasaki, H., Tsukita, Sh., and Furuse, M. (2004). JACOP, a novel plaque protein localizing at the apical junctional complex with sequence similarity to cingulin. J. Biol. Chem. *279*, 46014–46122.

Radice, G. L., Rayburn, H., Matsunami, H., Knudsen, K. A., Takeichi, M., and Hynes, R. O. (1997). Developmental defects in mouse embryos lacking N-cadherin. Dev. Biol. *181*, 64–78.

Rossant, J., and Cross, J. C. (2001). Placental development: lessons from mouse mutants. Nat. Rev. Genet. *2*, 538–548.

Saitou, M., Akatsuka-Ando, Y., Itoh, M., Furuse, M., Inazawa, J., Fujimoto, K. and Tsukita, Sh. (1997). Mammalian occludin in epithelial cells: its expression and subcellular distribution. Eur. J. Cell Biol. *73*, 222–231.

Saunders, D. N., Hird, S. L., Withington, S. L., Dunwoodie, S. L., Henderson, M. J., Biben, C., Sutherland, R. L., Ormandy, C. J., and Watts, C. K. (2004). Edd, the murine hyperplastic disc gene, is essential for yolk sac vascularization and chorioallantoic fusion. Mol. Cell Biol. *24*, 7225–7234.

Stevenson, B. R., Siliciano, J. D., Mooseker, M. S., and Goodenough, D. A. (1986). Identification of ZO-1, a high molecular weight polypeptide associated with the tight junction (zonula occludens) in a variety of epithelia. J. Cell Biol. *103*, 755–766.

Tsukita, Sh., Furuse, M., and Itoh, M. (2001). Multifunctional strands in tight junctions. Nat. Rev. Mol. Cell Biol. *2*, 285–293.

Umeda, K., Ikenouchi, J., Katahira-Tayama, S., Furuse, K., Sasaki, H., Nakayama, M., Matsui, T., Tsukita, Sa., Furuse, M., and Tsukita, Sh. (2006). ZO-1 and ZO-2 independently determine where claudins are polymerized in tight-junction strand formation. Cell *126*, 741–754.

Umeda, K., Matsui, T., Nakayama, M., Furuse, K., Sasaki, H., Furuse, M., and Tsukita, Sh. (2004). Establishment and characterization of cultured epithelial cells lacking expression of ZO-1. J. Biol. Chem. *279*, 44785–44794.

Willot, E., Balda, M. S., Fanning, A. S., Jameson, B., Van Itallie, C., and Anderson, J. M. (1993). The tight junction protein ZO-1 is homologous to the *Drosophila* discs-large tumor suppressor protein of septate junctions. Proc. Natl. Acad. Sci. USA *90*, 7834–7838.

Wittchen, E. S., Haskins, J., and Stevenson, B. R. (1999). Protein interactions at the tight junction. Actin has multiple binding partners, and ZO-1 forms independent complexes with ZO-2 and ZO-3. J. Biol. Chem. *274*, 35179–35185.

Xu, J., Kausalya, P. J., Phua, D. C., Ali, S. M., Hossain, Z., and Hunziker, W. (2008). Early embryonic lethality of mice lacking ZO-2, but not ZO-3, reveals critical and nonredundant roles for individual zonula occludens proteins in mammalian development. Mol. Cell Biol. *28*, 1669–1678.

Yamamoto, T., Harada, N., Kano, K., Taya, S., Canaani, E., Matsuura, Y., Mizoguchi, A., Ide, C., and Kaibuchi, K. (1997). The Ras target AF-6 interacts with ZO-1 and serves as a peripheral component of tight junctions in epithelial cells. J. Cell Biol. *139*, 785–795.

Yang, J. T., Rayburn, H., and Hynes, R. O. (1995). Cell adhesion events mediated by alpha 4 integrins are essential in placental and cardiac development. Development *121*, 549–560.

Zeigler, B. M., Sugiyama, D., Chen, M., Guo, Y., Downs, K. M., and Speck, N. A. (2006). The allantois and chorion, when isolated before circulation or chorio-allantoic fusion, have hematopoietic potential. Development *133*, 4183–4192.